Journal of Controlled Release 166 (2013) 147–158

Contents lists available at SciVerse ScienceDirect

Journal of Controlled Release

journal homepage: www.elsevier.com/locate/jconrel

NANOMEDICINE

Novel SN38 conjugate-forming nanoparticles as anticancer prodrug: *In vitro* and *in vivo* studies

Hongfang Zhang [a,b,1], Jinqiang Wang [a,1], Weiwei Mao [a], Jian Huang [c], Xianguo Wu [c], Youqing Shen [a], Meihua Sui [a,*]

[a] Key Laboratory of Biomass Chemical Engineering of Ministry of Education, Center for Bionanoengineering and State Key Laboratory of Chemical Engineering, Department of Chemical and Biological Engineering, Zhejiang University, Hangzhou, China, 310027
[b] Cancer Institute, Hangzhou Cancer Hospital, Hangzhou, China, 310002
[c] Cancer Institute (Key Laboratory of Cancer Prevention & Intervention, National Ministry of Education, Provincial Key Laboratory of Molecular Biology in Medical Sciences), The Second Affiliated Hospital, Zhejiang University School of Medicine, Hangzhou, China, 310009

ARTICLE INFO

Article history:
Received 6 June 2012
Accepted 12 December 2012
Available online 20 December 2012

Keywords:
CPT-11
SN38
Nanoparticles
Prodrug
Xenograft models

ABSTRACT

The clinical utility of CPT-11 is restricted by factors such as the low conversion rate to SN38, high interpatient variability and dose-limiting toxicity. SN38 is significantly more potent than CPT-11, but parental administration of SN38 is impossible due to its poor solubility and low stability. This study aimed to develop a novel SN38 prodrug (OEG-SN38) that may overcome the various drawbacks of CPT-11 and SN38 and be useful for clinics. We attached a very low molecular weight oligo (ethylene glycol) (OEG) chain selected as the hydrophilic part to hydrophobic SN38 *via* ester bond at the C20 position to form the amphiphilic OEG-SN38. In aqueous solution OEG-SN38 formed micelles with diameter of 28.74 ± 2.51 nm, and showed greatly improved drug loading, solubility and stability, with drug loading as high as 36% (wt.%). Moreover, these micelles were stable in PBS with only 4.71% SN38 released from the prodrug even after 35 h incubation, but released SN38 promptly by esterase hydrolysis. Most importantly, OEG-SN38 exhibited potent antitumor activity against a panel of human tumor cell lines, as well as favorable antitumor activity and high safety in human xenograft models. These encouraging data merit further preclinical and clinical investigation on this novel SN38 delivery system.

1. Introduction

CPT-11 (irinotecan or 7-ethyl-10[4-(1-piperidino)-1-piperidino]-carbonyloxy camptothecin) is an effective chemotherapeutic agent that induces cell death primarily by inhibiting the nuclear enzyme topoisomerase I (TOPI) [1]. It is widely prescribed for advanced colorectal cancer as a first- or second-line treatment [2,3]. However, the therapeutic effect and clinical utility of CPT-11 have been extremely restricted by several factors. First, CPT-11 itself has a very limited activity and exerts significant antitumor effect mainly by converting to its active metabolite SN38 (7-ethyl-10-hydroxy-camptothecin) *via* carboxylesterase (CE)-mediated de-esterification in the liver [4]. SN38 has 100–1000 fold more potent cytotoxicity *in vitro* compared with CPT-11 [5]. However, studies have shown that genetic and environmental factors influence CE activity by up to 10 folds [6]. The great interindividual difference of CE activity and the complexity of CPT-11 metabolism very likely lead to high interpatient variability in both efficacy and toxicity after administration of CPT-11. Besides, it is reported that only 2–8% of the administered dose of CPT-11 is converted to SN38 in humans [7]. This low conversion to SN38 results in low bioavailability of CPT-11 in patients. In addition, clinical results demonstrated that the pharmacologically important lactone ring of CPT-11 is readily converted to the inactive carboxylate form after infusion in humans or in the presence of human plasma albumin [8]. Another problem linked to CPT-11 clinical utility is its severe gastrointestinal toxicity and myelosuppression, which constitutes its dose limiting toxicity (DLT) [9].

Therefore, a significant clinical advantage could be gained from the direct administration of SN38, which would overcome the above drawbacks of CPT-11 in drug activation, metabolism and elimination. Nevertheless, SN38 cannot be administered directly, due to its extremely low water solubility in any physiologically compatible and pharmaceutically acceptable solvents. To exploit the full therapeutic potential of SN38, a number of drug delivery systems, *e.g.* PEGylation conjugate, polymer micelle, liposome formulation, dendrimers, have been extensively investigated to improve water-solubility and bioavailability of SN38 [10–13]. Unfortunately, some inherent drawbacks are associated with these drug delivery systems, especially low drug loading and premature burst release. For example, polymer conjugate of SN38 EZN-2208 has a payload of only 3.7% (weight ratio of SN38 molecular

* Corresponding author at: Department of Chemical and Biological Engineering, Zhejiang University, Hangzhou, China, 310027. Tel./fax: +86 571 87951493.
E-mail address: suim@zju.edu.cn (M. Sui).
[1] Equal contribution.

0168-3659/$ – see front matter © 2012 Elsevier B.V. All rights reserved.
http://dx.doi.org/10.1016/j.jconrel.2012.12.019

to the entire polymer conjugate) even though four SN38 moleculars were conjugated to the PEG backbone [10]. Low drug loading may significantly limit the clinical application because repeated administration of a large amount of inactive carriers into patients may induce systemic toxicity [14]. Drug-entrapped liposomal formulation, as another common drug carrier, also suffers from many problems such as low stability under physiological conditions, batch to batch irreproducibility, low entrapment efficiency and difficulties in controlling liposome size [15].

We have recently developed a self assembling prodrug approach to fabricate high drug loading nanocarriers [14,16]. In the present study, we synthesized a novel self-assembling SN38 prodrug aiming to develop a drug delivery system potentially overcoming the above limitations and useful for clinics. A very low molecular weight oligo(ethylene glycol) (OEG) chain selected as the hydrophilic part was attached to hydrophobic SN38 *via* ester bond at the C20 position of SN38. This surfactant-like amphiphilic molecular (named as OEG-SN38) is expected to form micelles in aqueous solution, which should substantially enhance the water solubility as well as the tumor targeting ability of SN38 *via* EPR (enhanced permeability and retention) effect of tumor. Meanwhile, the very low molecular weight of OEG portion and the relatively stable chemical linkage between OEG and SN38 would significantly increase the efficacy and stability of drug loading. In addition, acylation of the C20-hydroxy of SN38 was evidenced to assist in preserving SN38 in the active lactone form [17]. The successful synthesis of OEG-SN38 was confirmed, its physiochemical properties were characterized, and its biological activities were investigated *in vitro* and *in vivo* with appropriate animal models. Our data demonstrated that this novel SN38-conjugate has greatly improved water solubility and stability, with drug loading as high as 36% (wt.%). Particularly, OEG-SN38 exhibits excellent *in vitro* and *in vivo* antitumor activity and safety, holding the promise to become a new and potent anticancer drug.

2. Materials and methods

2.1. Agents, cell lines and animals

SN38 was purchased from Xi'an Sendflld Science and Technology (Xi'an, China). Irinotecan hydrochloride was from Chengdu Yuancheng Biotechnology Co. (Chengdu, China). 1, 2-ethanedithiol (98%) (EDT) was purchased from Aladdin (Shanghai, China). Oligo(ethylene glycol) methyl ether acrylate (OEGMEA, Mn: 480) was received from Aldrich (St Louis, USA). Other reagents were purchased from Sinopharm Chemical Reagent Co. (Shanghai, China). MCF-7 (human breast carcinoma), KB (human epidermoid carcinoma), HT-29 (human colorectal carcinoma) and SKOV-3 (human ovarian carcinoma) cell lines were obtained from American Type Culture Collection and maintained in our laboratory. MCF-7, KB, SKOV-3 and BCap37 (human breast carcinoma) cell lines have been used in our previous studies [18–20]. Both 6–8-week-old female BALB/c homozygous athymic nude mice and ICR strain mice were purchased from the Animal Center of Zhejiang University, and maintained under standard conditions. Use of animals for *in vivo* studies was approved by the Animal Ethics Committee in Zhejiang University.

2.2. Preparation of OEG-SN38 conjugate

2.2.1. Synthesis of OEG-SH

10 g (20.8 mmol) OEGMEA and 10 g (106 mmol) EDT were mixed together and 0.5 mL Et_3N was added as catalyst. After stirring overnight at room temperature, the mixture was poured into 50 mL water, and HCl was added to neutralize the solution. After three washes with 100 mL hexane, the water was removed under vacuum, and pure OEG-SH (8 g, yield 80%), as characterized by ^1H NMR spectroscopy (Fig. S1), was obtained.

2.2.2. Synthesis of Boc-SN38

1 g (2.5 mmol) SN38 and 1 g (4.5 mmol) Di-tert-butyl dicarbonate were dissolved in CH_2Cl_2 and 5 mL pyridine was used as a catalyst. After stirring for 3 h at room temperature, the reaction mixture was washed by aqueous hydrochloric acid solution and then dried over anhydrous $MgSO_4$ to obtain 1.2 g Boc-SN38 in 90% yield, as characterized by ^1H NMR spectroscopy (Fig. S2).

2.2.3. Synthesis of Boc-SN38MA

1.25 g (2.5 mmol) Boc-SN38 was dissolved in 100 mL anhydrous CH_2Cl_2, and 0.69 mL (5 mmol) Et_3N was added as HCl acceptor. Under stirring in ice bath, 0.41 mL (5 mmol) acryloyl chloride was added dropwise into the mixture. After stirring for 2 h, 1 g of the desired Boc-SN38MA was obtained by passing through a chromatographic column (20:1, CH_2Cl_2/MeOH) in 70% yield, as characterized by 1H NMR spectroscopy (Fig. S3).

2.2.4. Synthesis of OEG-SN38

1.1 g (2 mmol) OEG-SH and 1.14 g (2 mmol) Boc-SN38MA were dissolved in 10 mL CH_2Cl_2 and 0.5 mL Et_3N was added as catalyst. After stirring overnight at room temperature, Et_3N was washed away by HCl and the solution was then dried with $MgSO_4$. To deprotect Boc groups, 30% TFA was added to the filtered clear solution and stirred for 2 h. Deionized water was used to wash TFA away, and the solution was then dried and filtered. CH_2Cl_2 was removed under vacuum to give the final product of OEG-SN38 in 70% yield (1.5 g), as characterized by ^1H NMR spectroscopy (Fig. S4) and ^{13}C NMR spectroscopy (Fig. S5).The reaction route is shown in Fig. 1A.

2.3. Micelle formation and determination of critical micelle concentration (CMC)

OEG-SN38 dissolved in THF was added dropwise into 0.01 M PBS under stirring. After stirring for 2 h, THF was removed under vacuum, and the residual solution was the desired micelle-based OEG-SN38. The initial micelle solution was diluted with 0.01 M PBS to obtain the required solutions for further studies. To determine the CMC of OEG-SN38, a known amount of Nile Red in CH_2Cl_2 was added to a series of vials. When CH_2Cl_2 was evaporated, a measured amount of OEG-SN38 solution was added to each vial to obtain a final concentration of 1 μM Nile Red and stirred overnight in dark. The fluorescence emission intensity was measured at the wavelength of 620 nm (excited at 543 nm) using a microplate reader (Molecular Devices, SpectraMAX M2e, USA). CMC was determined at the intersection of the tangents to the two linear portions of the curve of the fluorescence intensity as a function of OEG-SN38 concentration [14].

2.4. Hydrolysis of OEG-SN38 and CPT-11 detected by HPLC

The hydrolysis of OEG-SN38 (200 μg/mL) in PBS (pH 7.4) was detected by high-performance liquid chromatography (HPLC, Waters, Singapore). Furthermore, according to our previous studies [14], 5 U and 10 U esterase solutions were used to study the effect of esterase on the hydrolysis of OEG-SN38 (200 μg/mL) and CPT-11 (200 μg/mL). Briefly, the OEG-SN38 or CPT-11 solution was incubated in a 37 °C shaker. At specific time intervals, samples (0.1 mL) were withdrawn and analyzed by HPLC using a SunFire™ C18 column (4.6×250 mm, 5 μm) at 35 °C. A gradient elution method of 60–95% methanol/water was applied at a flow rate of 1 mL/min. During assays, 20 μl of each sample was injected into the analytic column. The release of SN38 was detected by UV at 360 nm, and the hydrolysis was determined based on the ratio of SN38 peak areas to the corresponding OEG-SN38 or CPT-11 peak areas.

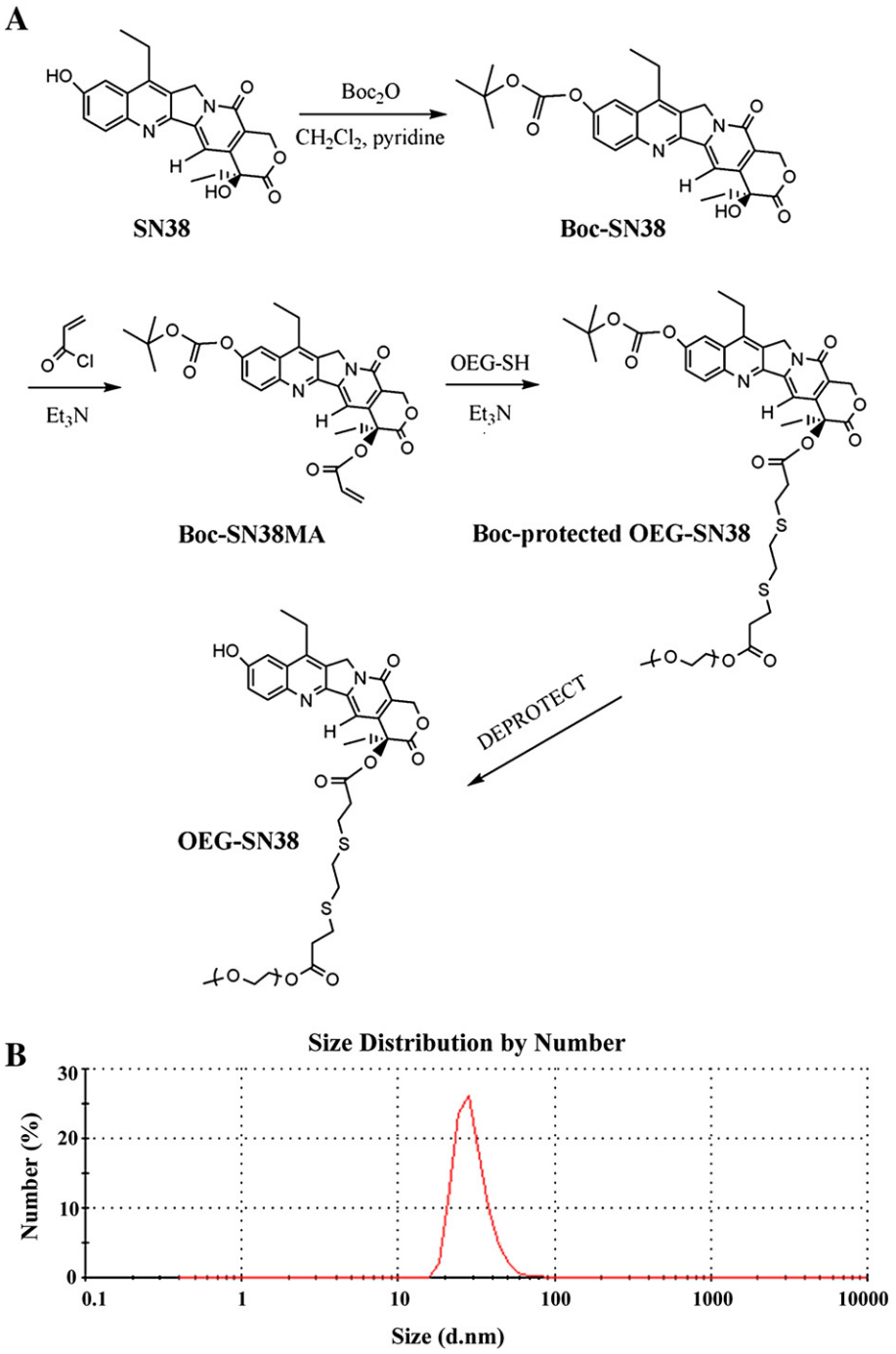

Fig. 1. Synthesis (A) and size distribution (B, in PBS as detected by DLS) of OEG-SN38.

2.5. Stability of OEG-SN38 nanoparticles in human plasma

To investigate whether OEG-SN38 nanoparticles could remain stable in blood circulation, and thereby profit from the EPR effect, we further incubated OEG-SN38 (200 μg/mL) in human plasma *in vitro*. Samples (1 mL) were withdrawn at 0 h, 12 h, 24 h and 36 h, respectively, and analyzed by dynamic light scattering (DLS, Malvern Zen3600, UK).

2.6. Cellular uptake of OEG-SN38 nanoparticles

Tumor cells were plated onto glass-bottom petri dishes in 1.5 mL of complete culture medium for 24 h before treatment. Cells were exposed to OEG-SN38 loaded with Nile Red and incubated for 2 h at final SN38 concentration of 16.96 μg/mL. Then the solution was replaced with fresh medium, and the cells were further incubated with LysoTracker (Molecular Probes, USA) at a concentration of 200 nM for 1.5 h to label lysosomes. The images were then taken using a confocal laser scanning microscope (CLSM, Nikon-A1 system, Japan). LysoTracker was observed using a 488-nm laser, and the emission wavelength was read from 510 to 540 nm and expressed as green. OEG-SN38 loaded with Nile Red was observed using a 543 nm laser, and the emission wavelength was read from 560 to 610 nm and expressed as red.

2.7. 3-(4,5-Dimethylthiazol-2-yl)-2,5-diphenyltetrazolium bromide (MTT) assay

The cytotoxicity of OEG-SN38 was determined by MTT assay in a large panel of human tumor cell lines including BCap37, MCF-7, HT-29, SKOV-3 and KB. Briefly, adherent cells (4000–5000 cells per well) were evenly plated into 96-well plates and incubated overnight. Then cells were exposed to serial dilutions of OEG-SN38, SN38 or CPT-11 and further incubated for 48 h. Subsequently, the medium in each well was replaced with fresh culture medium containing 1 mg/mL MTT. The plates were incubated for additional 3 h, allowing viable cells to reduce the yellow tetrazolium salt (MTT) into dark blue formazan crystals. Finally, DMSO was added to dissolve the formazan crystals. The absorbance was determined at 562 nm with a microplate spectrophotometer (Molecular Devices, SpectraMax M2e, USA). Each drug concentration was tested in triplicate and in three independent experiments.

2.8. Cell cycle analysis

Cell cycle distribution and regulation were monitored by flow cytometric analysis. Tumor cells were exposed to a range of concentrations of SN38, OEG-SN38 and CPT-11. Cell sample preparation was done as described previously [19,21]. Briefly, at the end of each time point, all cells were harvested and fixed in 70% ethanol diluted in PBS, followed by incubation in PBS containing 100 μg/mL RNase and 40 μg/mL propidium iodide before flow cytometry analysis. Cell cycle distribution and DNA content were determined using FACScan (BD, USA).

2.9. Acute toxicity studies in mice

The acute toxicity of OEG-SN38 was studied in ICR strain mice with the initial body weight of 19–22 g. Mice were randomly divided into five groups of ten (five males and five females) and maintained under standard conditions, with free access to food and water. After a one-week acclimation period, OEG-SN38 conjugate was delivered intravenously to each group of mice at doses of 200, 170, 144.5, 123, 105 mg/kg, respectively, according to the data obtained from preliminary studies. Animals were observed every 1–2 h on the treatment day, twice a day later, for up to 14 days post drug treatment. The intoxication symptoms, changes in body weight and the time of death of treated mice were recorded in detail. The half lethal value LD_{50} and 95% confidence interval (CI) were calculated by modified Karber's method.

2.10. In vivo antitumor efficacy

To develop the human tumor xenografts, *in vitro* growing BCap37 and SKOV-3 cells were harvested by exposure to trypsin-EDTA, washed with PBS and implanted into the right flanks of mice [20]. When BCap37 and SKOV-3 tumors had reached a mean diameter of around 0.5 cm, mice were assigned to five treatment groups ($n=4$/group): (a) CTL (PBS); (b) CPT-11 at 7.94 mg/kg (equivalent to 5 mg/kg SN38);(c) OEG-SN38 at 13.89 mg/kg (equivalent to 5 mg/kg SN38); (d) CPT-11 at 15.88 mg/kg (equivalent to 10 mg/kg SN38) and (e) OEG-SN38 at 27.78 mg/kg (equivalent to 10 mg/kg SN38). The treatment regimens were initiated on day 1 (*i.v.*), repeated every 2 days for a total of 6 cycles. After the Medication Phase (Day 1–11), the animals were left untreated for a few days (defined as Withdrawal Phase) until they were terminated. Tumor volume (mm^3) was calculated using the following formula: $V(mm^3)=A(mm)\times B(mm)^2/2$, where A and B were the longest and widest diameter of tumor, respectively. At the end of the experiments, all animals were sacrificed according to institutional guidelines. Tumors were resected, weighed, and fixed in formalin for paraffin embedding. Inhibition rates (IR) of tumor growth were calculated using the following equation: IR = 100% × (mean tumor weight of control group − mean tumor weight of experimental group)/mean tumor weight of control group [20]. Data are representatives of two independent experiments.

2.11. Histological examination of tumor tissues

The removed xenograft tumors were fixed with 4% neutral buffered paraformaldehyde and embedded in paraffin before making tissue sections. Four micrometer tissue sections were prepared and stained with hematoxylin and eosin (H&E, Fisher Scientific, USA) for histological examinations. The histological identification of apoptotic cells has been described and illustrated in our previous publications [20].

2.12. Statistical analysis

Data are presented as means ± standard errors. Tumor volumes over time were analyzed by one-way ANOVA (analysis of variance) and subsequently by Student's *t*-test [20]. All other statistical analyses were performed using Student's *t*-test. Differences were considered statistically significant at a level of $p<0.05$.

3. Results

3.1. Preparation and characterization of OEG-SN38 nanoparticles

SN38 contains active phenolic and less active C20 hydroxy groups. To selectively acylate the 20-OH, we firstly protected the phenol group with Boc, and then tried to introduce the acrylate to 20-OH. In brief, SN38 was first reacted with methacrylic anhydride in the presence of DAMP. However, many side reactions occurred and purification was quite complicated. We then tried acryloyl chloride instead of methacrylic anhydride due to its higher reactivity. The reaction could not take place when *N, N-diisopropylethylamine* was used as HCl acceptor. With Et_3N as HCl acceptor, the reaction went well as expected. The pure OEG-SN38 was obtained after chromatographic purification (20:1, H_2Cl_2/MeOH) in a 70% yield.

OEG-SN38 formed nanoparticles with a hydrodynamic diameter of 28.74 ± 2.51 nm (Fig. 1B), and the CMC value detected by the method described above was 60 μg/mL, as shown in Fig. 2A. Moreover, OEG-SN38 nanoparticles had a fixed drug loading content of as high as 36% (wt.%). Very importantly, these nanoparticles slowly released SN38 in PBS (pH 7.4), with only 4.71% of SN38 released even after 35 h incubation, suggesting that OEG-SN38 has no premature burst release (Fig. 2B), which is a general problem for most nanoparticle drug carriers. However, in the presence of 10 U esterase, up to 54.9% of SN38 was released from its prodrug after only 24 h incubation (Fig. 2B). Although 5 U esterase showed less effect on the hydrolysis of OEG-SN38 than 10 U esterase, there was still around 12% of SN38 released from its prodrug after 24 h incubation. In contrast, no SN38 was released from CPT-11, even after 48 h incubation in 10 U esterase solution. Furthermore, OEG-SN38 was found to be stable in the form of nanomicelle during the longtime incubation in human plasma (Fig. 3).

3.2. Cellular uptake and intracellular localization of OEG-SN38 nanoparticles

OEG-SN38 nanoparticles were labeled by Nile Red and their cellular uptake and intracellular localization in cancer cells were observed by CLSM. The representative results are depicted in Fig. 2C. After 2 h incubation at 37 °C, OEG-SN38 nanoparticles were quickly taken up by SKOV-3 cells. Overlay of the images taken from LysoTracker, Nile Red and Transmittance channels demonstrated that OEG-SN38 was mostly localized in lysosomes (yellow spots, in Fig. 2C-c). Some conjugates not associated with lysosomes (red spots, in Fig. 2C-c) were probably those that had already escaped from the lysosomes within the 2 h incubation.

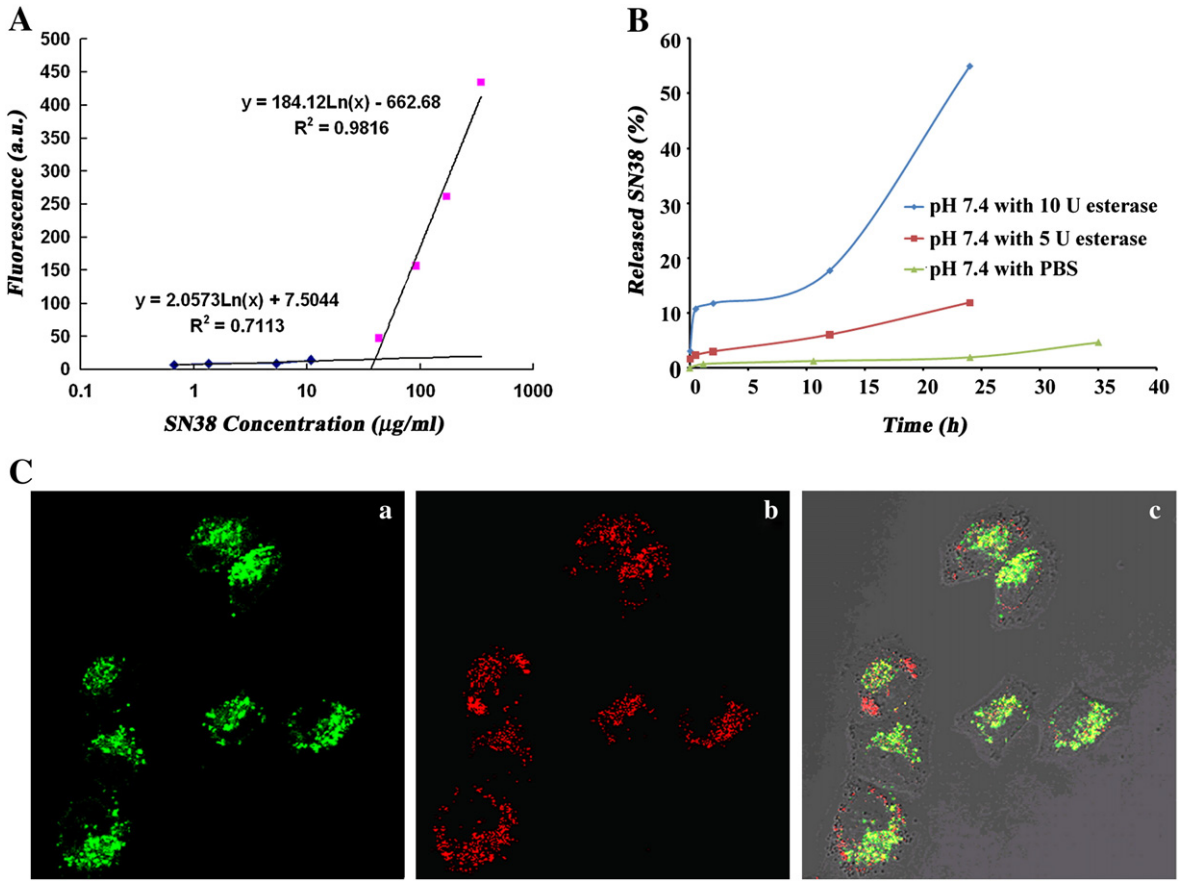

Fig. 2. CMC, SN38 release kinetics from the OEG-SN38 nanoparticles, and cellular localization of OEG-SN38. A, the CMC value of OEG-SN38 was 60 μg/mL. B, SN38 release kinetics was determined in PBS at pH 7.4 and 37 °C, with or without 5 U or 10 U esterase for indicated time. C, the subcellular localization of Nile Red-loaded OEG-SN38 nanoparticles into SKOV-3 cells was observed by CLSM after 2 h incubation, (A) LysoTracker channel (green, to label lysosomes), (B) Nile Red channel (red, to label OEG-SN38), and (C) overlap of LysoTracker, Nile Red and Transmittance channels.

3.3. In vitro cytotoxicity

OEG-SN38 nanoparticles demonstrated significant *in vitro* antitumor activity comparable to SN38 dissolved in DMSO, but far better than CPT-11, against a large panel of human tumor cell lines, including SKOV-3, MCF-7, BCap37, HT-29 and KB (shown in Fig. 4). The IC_{50} (concentration inhibiting cell growth to 50% of control) values of OEG-SN38 in above cell lines were 0.032, 0.27, 0.30, 1.61, 1.61 μg/mL, respectively, being around 2-fold higher than that of SN38 in SKOV-3, MCF-7, HT-29 and KB cell lines, and around 5-fold higher than that of SN38 in BCap37 cell line. These data indicate that OEG-SN38 released SN38 sufficiently after taken up by cancer cells. In all the five cell lines tested, OEG-SN38 exhibited significantly higher antitumor activity than CPT-11. For instance, the IC_{50} values of CPT-11 against the tested cell lines were 6.53, 4.41, 21.65, 49.65, and 18.29 μg/mL, respectively, which were 11.3–199.8 fold higher than that of OEG-SN38.

3.4. Cell cycle analysis

As summarized in Fig. 5, our data showed that at 24 h, there were 14.94%, 16.34% and 42.55% of tumor cells arrested at G2/M phase, respectively, after the administration of 0.016, 0.032 and 0.08 μg/mL OEG-SN38, all of which were significantly higher than that of the control group (9.52%). To a much less extent, CPT-11 incubation for 24 h with corresponding concentrations only induced 11.97%, 12.49% and 12.86% of cells in G2/M phase, respectively. At 48 h, treatment of OEG-SN38 continuously arrested tumor cells at the G2/M phase of the cell cycle. However, the G2/M populations in groups treated with various concentrations of CPT-11 decreased and recovered to the similar level as the control group. When exposed to free SN38, SKOV-3 cells were arrested in both S and G2/M phases of the cell cycle, indicating that tumor cells were more sensitive to SN38 than OEG-SN38 and CPT-11. These data was consistent with the above MTT results showing that free SN38 exhibited relatively higher *in vitro* antitumor activity than OEG-SN38, both of which were far better than CPT-11 *in vitro*.

3.5. Acute toxicity of OEG-SN38 nanoparticles

As expected, single intravenous injection of OEG-SN38 nanoparticles induced acute toxicity in ICR mice in a dose-dependent fashion (Table 1). Intoxication symptoms such as reduction in voluntary movement, irregular respiration, motoric disturbances and even rapid death were observed in some animals after drug exposure. The earliest and the latest intoxication-related death appeared within one minute and three hours after dosing, respectively. Intoxication symptoms disappeared 24 h after drug administration in survival animals, and physiological function, food consumption and body weight gains of the mice were recovered. The LD_{50} value and 95% confidence interval (CI) of OEG-SN38 were 151.36 mg/kg and 138.29–165.65 mg/kg, respectively.

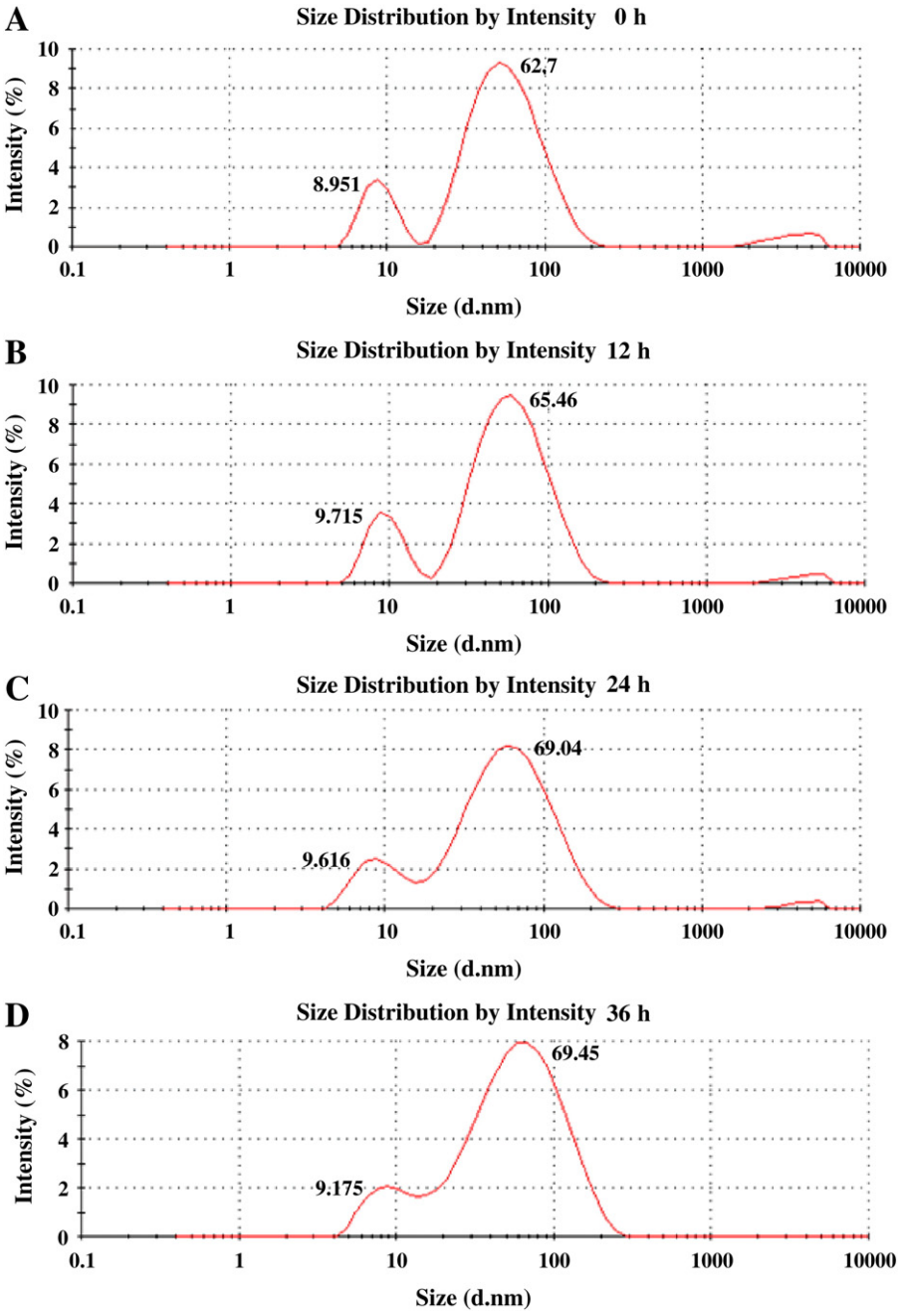

Fig. 3. Stability of OEG-SN38 nanoparticles in human plasma. OEG-SN38 was incubated in human plasma for 0 h, 12 h, 24 h and 36 h, respectively. Samples were withdrawn and analyzed by DLS. The left and right peaks in panel A–D represent plasma protein alone and OEG-SN38 nanoparticles binding to plasma protein, respectively.

3.6. In vivo antitumor activity in human breast xenograft tumors

Encouraged by the above *in vitro* data, we further evaluated the *in vivo* antitumor efficacy of OEG-SN38 with BCap37 xenograft model. OEG-SN38 and CPT-11 were administered *i.v.* at defined doses with an intermittent q2d×6 schedule, and the control group was treated with PBS *via* the tail vein. Our data demonstrated that OEG-SN38 and CPT-11 both effectively repressed BCap37 tumor growth (all $p<0.005$, in comparison with control group, Fig. 6A). During the Medication Phase, there was a statistical difference on the tumor volume between groups treated with 13.89 mg/kg of OEG-SN38 and 7.94 mg/kg of CPT-11 (both equivalent to 5 mg/kg SN38, $p<0.05$). However, this statistical difference disappeared in the Withdrawal Phase ($p>0.05$). This finding was further confirmed when the doses of OEG-SN38 and CPT-11 increased to 27.78 mg/kg and 15.88 mg/kg (both equivalent to 10 mg/kg SN38), respectively, as no statistical difference on tumor volume was observed in either Medication Phase or Withdrawal Phase (both $p>0.05$). Meanwhile, all the tumors were collected for the calculation of IR at the end of the experiments. The overall IRs of low dosage OEG-SN38 and CPT-11 were 72.51%±4.97% and 83.09%±7.53%, respectively ($p>0.05$), and those for high dosage OEG-SN38 and CPT-11 were 89.23%±3.68% and 96.23%±1.65%, respectively ($p<0.05$) (Fig. 6D). Body weight of all animals increased steadily throughout the study (Fig. 6B) and no toxic

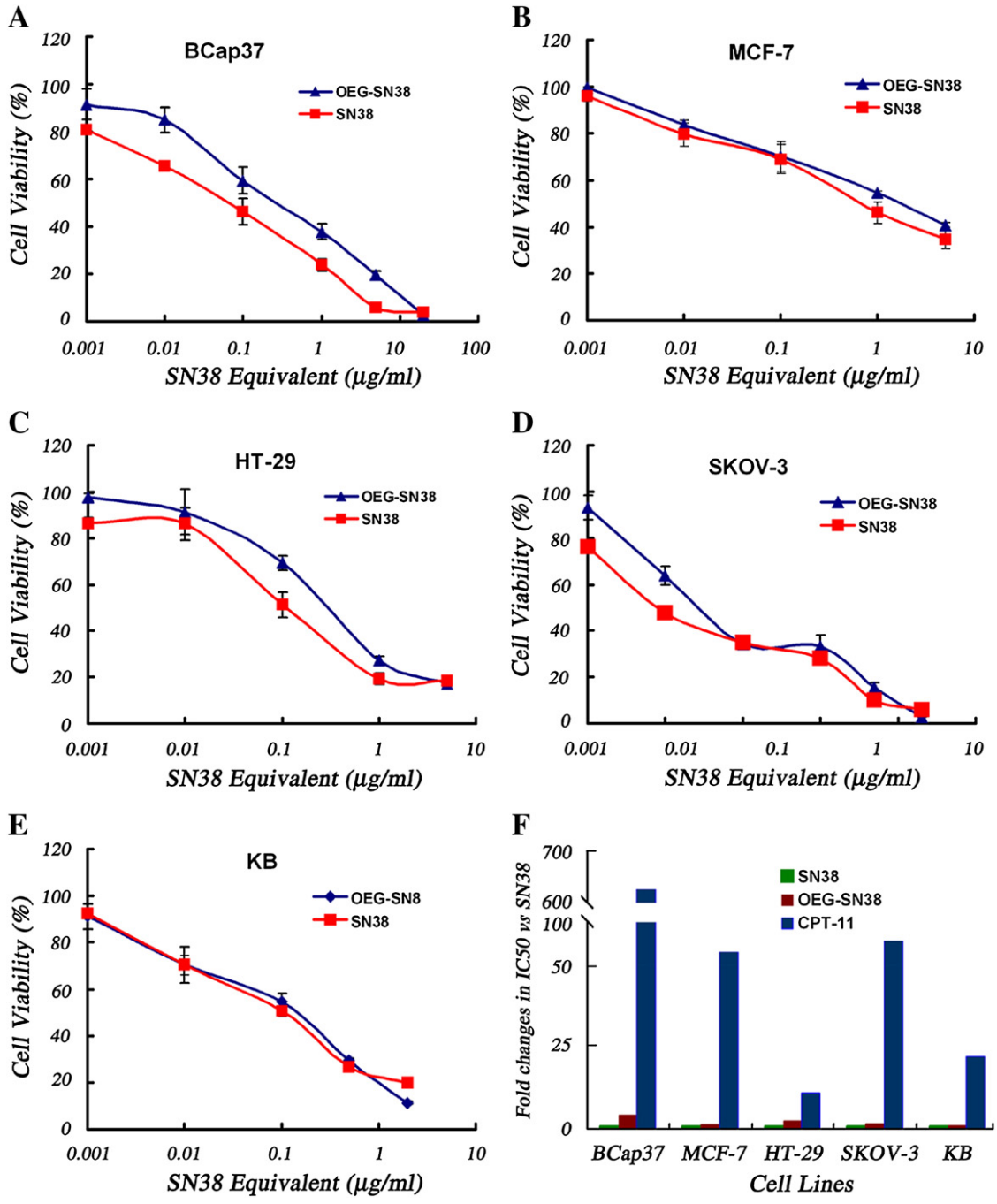

Fig. 4. *In vitro* cytotoxicity of SN38, OEG-SN38 and CPT-11. A–E, the antitumor activity was determined by MTT assay after indicated tumor cell line was treated with various concentrations of different drug for 48 h. Untreated cells were used as controls. Cell viability was calculated as the absorbance ratio of treated to control groups. F, the IC_{50} values were calculated and presented as ratios to SN38 dissolved in DMSO. Data were presented as Mean ± S.E.

characteristics were observed. These data indicate that OEG-SN38 was well-tolerated and exerted excellent therapeutic activity in nude mice bearing BCap37 xenograft tumors (Fig. 6C).

3.7. *In vivo* antitumor activity in human ovarian xenograft tumors

Moreover, we further evaluated the *in vivo* antitumor potency of OEG-SN38 conjugate with SKOV-3 human ovarian cancer xenograft model. We found that administration of 27.78 mg/kg OEG-SN38 and 15.88 mg/kg CPT-11 (both equivalent to 10 mg/kg SN38, q2d × 6, *i.v.*) significantly repressed tumor growth in mice (both $p<0.05$, in comparison with control group, Fig. 7A and B). No matter in Medication Phase or Withdrawal Phase, no statistical difference on tumor volume was observed between mice treated with OEG-SN38 and CPT-11 (both $p>0.05$). However, when the animals were terminated, the overall IRs of OEG-SN38 and CPT-11 were 70.03% ± 6.30% and 84.95% ± 6.54%, respectively ($p<0.05$, Fig. 7B). Similar to the findings observed in BCap37 xenograft model, body weight of all the SKOV-3-tumor bearing mice increased steadily throughout the study and no toxic characteristics were observed (data not shown). These data indicate that OEG-SN38 exerted significant therapeutic activity in nude mice bearing SKOV-3 xenograft tumors.

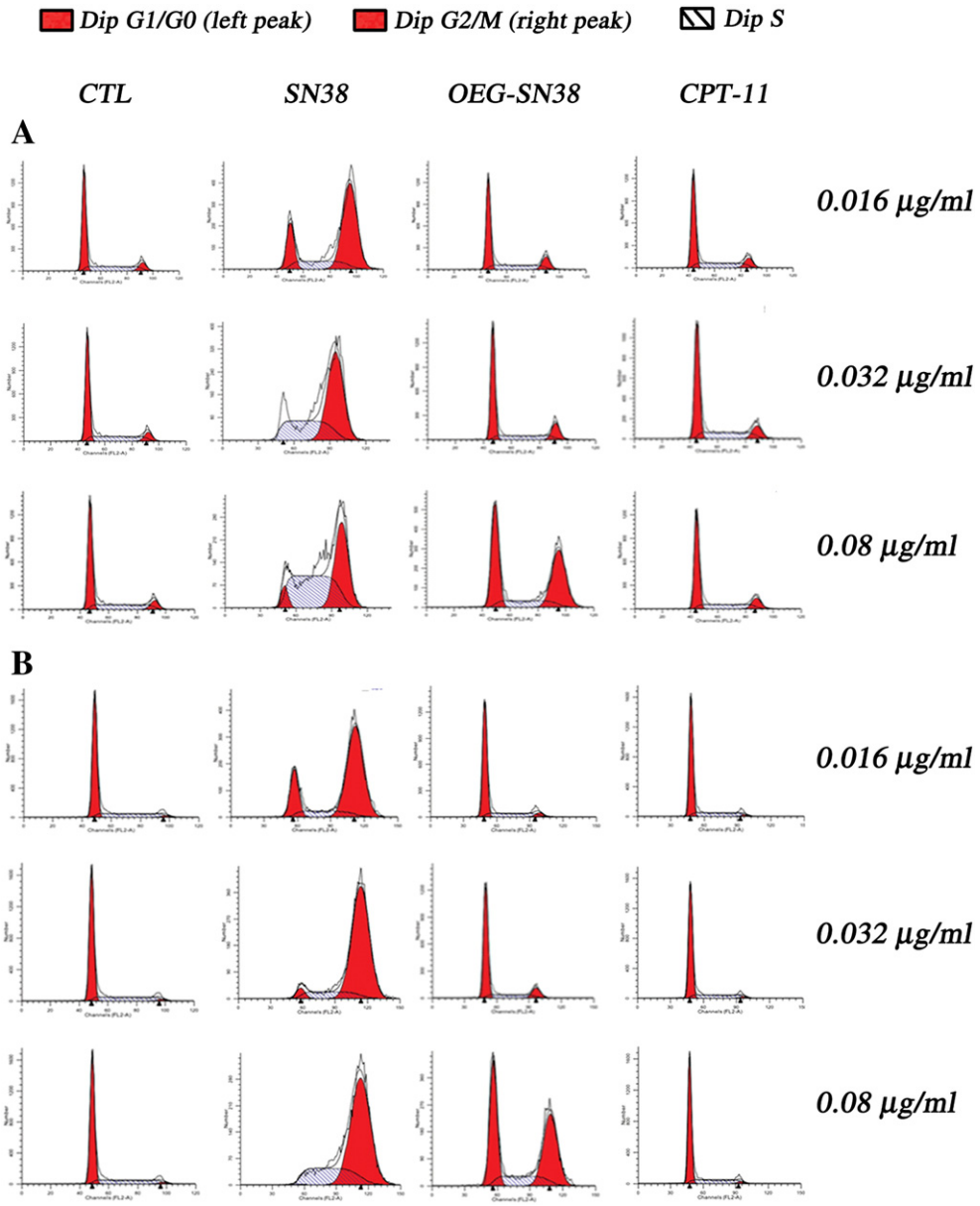

Fig. 5. Flow cytometric analysis of cell cycle distribution. SKOV3 cells exposed to SN38 (dissolved in DMSO), OEG-SN38 or CPT-11 for 24 h and 48 h, respectively, were harvested. DNA content was stained with propidium iodide for flow cytometric analysis. Peaks corresponding to G1/G0, G2/M, and S phases of the cell cycle were indicated.

3.8. Histological analysis of xenograft tumors

To obtain more complete insight into the inhibitory effect of OEG-SN38 on human xenograft tumors, histological studies on tumor tissue sections with H&E staining were conducted. As shown in Fig. 7C, in the control groups, both BCap37 and SKOV-3 tumor tissue sections were composed of tightly packed tumor cells interspersed with various amounts of stroma (a, d, g). However, in tumors treated with either CPT-11 (Fig. 7C-b, e, h) or OEG-SN38 (Fig. 7C-c, f, i), the histological features of xenograft tumors exhibited significant differences from the corresponding control groups. For instance, tumor cells with enlarged sizes and excessive vacuolization were seen in BCap37 tumor tissue sections after the treatment of CPT-11 or OEG-SN38. Additionally, many of the tumor cells exhibited typical apoptotic characteristics; That is, they were composed of membrane-bound, small nuclear fragments surrounded with a rim of cytoplasm [20]. The histological features were quite similar in tumors treated with either CPT-11 or OEG-SN38 (Fig. 7C) at equivalent dose level, which was consistent with the above data that both compounds possess significant anticancer activity in tested xenograft models.

Table 1
Acute toxicity of OEG-SN38 in ICR mice upon *i.v.* administration.

Dose of OEG-SN38 (mg/kg)	No. of mice tested	No. of dead mice	Mortality (%)
200.0	10	10	100
170.0	10	7	70
144.5	10	4	40
123.0	10	0	0
105.0	10	0	0

4. Discussion

In the past decades, nanostructures of anticancer drugs have been proven to be innovative and promising in cancer chemotherapy for their inherent advantages over traditional small molecular drugs

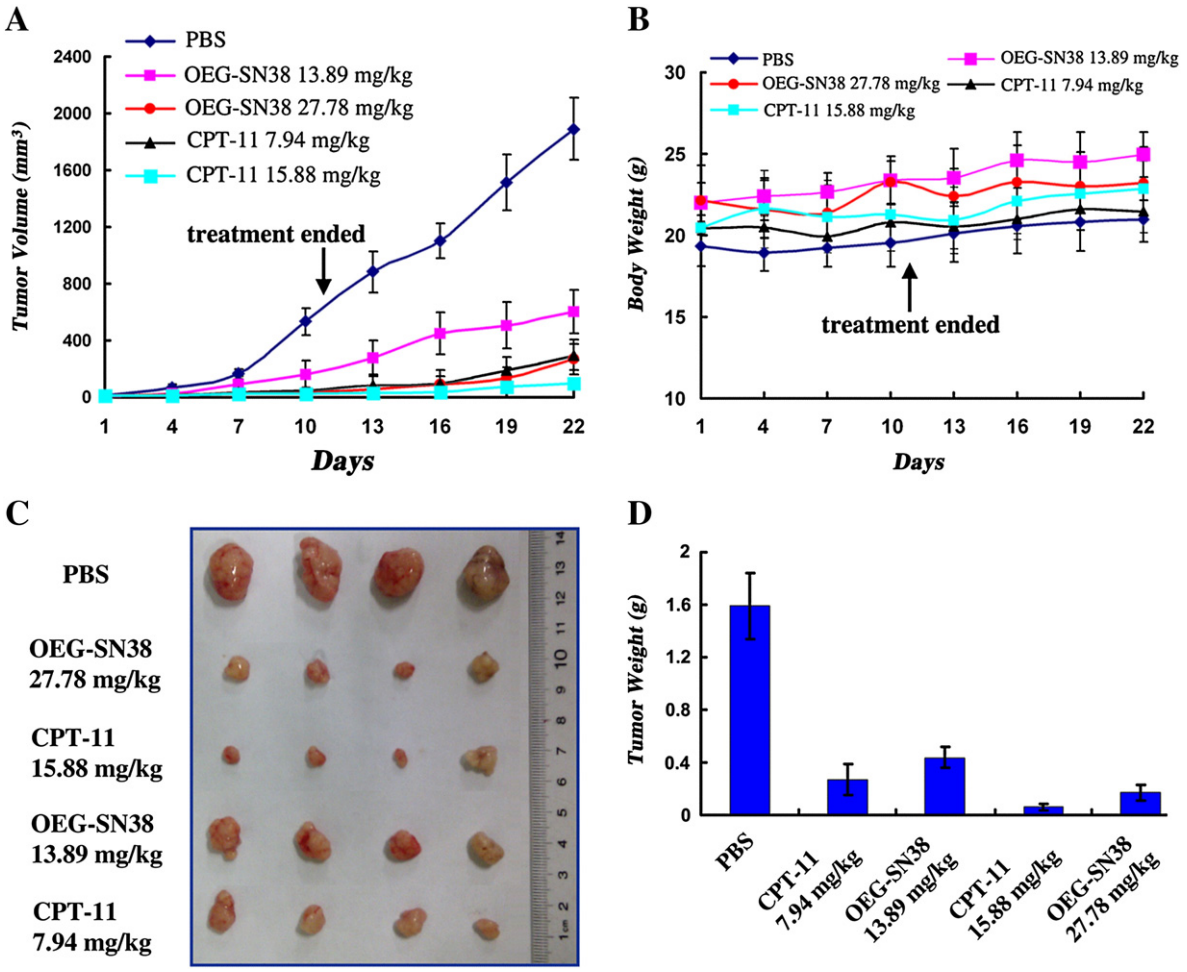

Fig. 6. Therapeutic effects of OEG-SN38 and CPT-11 against BCap37 human breast xenograft tumors. Nude mice bearing BCap37 tumors were treated with PBS, OEG-SN38 or CPT-11 at indicated doses (q2d × 6). 13.89 mg/kg OEG-SN38 and 7.94 mg/kg CPT-11 were equivalent to 5 mg/kg SN38. 27.78 mg/kg OEG-SN38 and 15.88 mg/kg CPT-11 were equivalent to 10 mg/kg SN38. A, determination of tumor volume. B, body weight changes of the mice. C, photos of tumors upon animal termination. D, tumor weight upon animal termination. Data were presented as Mean ± S.E.

[22,23]. Herein, we successfully prepared a novel OEGylated self-assembling SN38 prodrug (OEG-SN38) to overcome the various drawbacks of free SN38, such as low water solubility and low bioavailability, as well as to overcome the various disadvantages of CPT-11 in drug activation, metabolism and elimination. It is known that nanoparticles less than 20 nm may escape renal clearance while those larger than 150 nm are more likely uptaken by liver and spleen [24]. Therefore, the favorable size of OEG-SN38 nanoparticles (28.74 ± 2.51 nm) and their proven stability in blood circulation may assist in preventing sequestration by RES (reticuloendothelial system) and targeting tumor sites passively *via* the EPR effect [25–27]. Meanwhile, acylation of the 20-hydroxy could preserve SN38 in the active closed lactone form essential for its activity during circulation [17], which might also potentiate its antitumor activity. Furthermore, the very low molecular weight of OEG portion dramatically increased the drug loading efficacy of OEG-SN38 to 36% (wt.%), which is significantly higher than all other reported SN38-containing drug delivery systems (mostly around 10%) [10,11,13,24]. This high and stable drug loading would significantly reduce the amount of inactive carriers into patients and thereby reduce the systemic toxicity. On the other hand, although gene-directed enzyme/prodrug therapy (GDEPT) was recently demonstrated to improve the antitumor activity of CPT-11 or SN38, the preparation of these systems are much more complicated than OEG-SN38 [28–30].

Esterases are known to be abundant in the cell cytosol and lysosomes. Thus, the ester linkage between OEG and SN38 would be stable during transport in the blood circulation and thereby help eliminate the premature burst release of active drug. Once enter the cells, the ester linkage will be easily cleaved upon exposure to intracellular esterase for release of free SN38, which may further enhance the tumor targeting ability of OEG-SN38. Indeed, our data showed that OEG-SN38 was quite stable in PBS, with only 4.71% of SN38 released even after 35 h incubation, which is far better than other reported nanosized SN38-prodrugs that may release even more than 50% of SN38 after 24 h incubation in PBS. However, in 10 U esterase solution, up to 54.9% of SN38 was released from OEG-SN38 after 24 h incubation while no SN38 was converted from CPT-11 in esterase solution even after 48 h incubation. These results demonstrated that OEG-SN38 releases SN38 in a controlled esterase-responsive fashion, and may overcome the disadvantage of CPT-11 on reliance of carboxylesterase which is mainly present in liver in humans and has great interspecies and individual variability.

SN38 targets the nuclear enzyme TOPI, and acts by binding covalently to the reversible DNA-TOPI complexes during DNA replication, RNA transcription and DNA repair, thereby inducing irreversible double-bond DNA damage [31]. These pharmacological events of SN38 ultimately lead to cell cycle arrest at G2/M and S phases or cell death [32]. In the present study, we found that OEG-SN38 prodrug had potent *in vitro* antitumor activity, similar to SN38

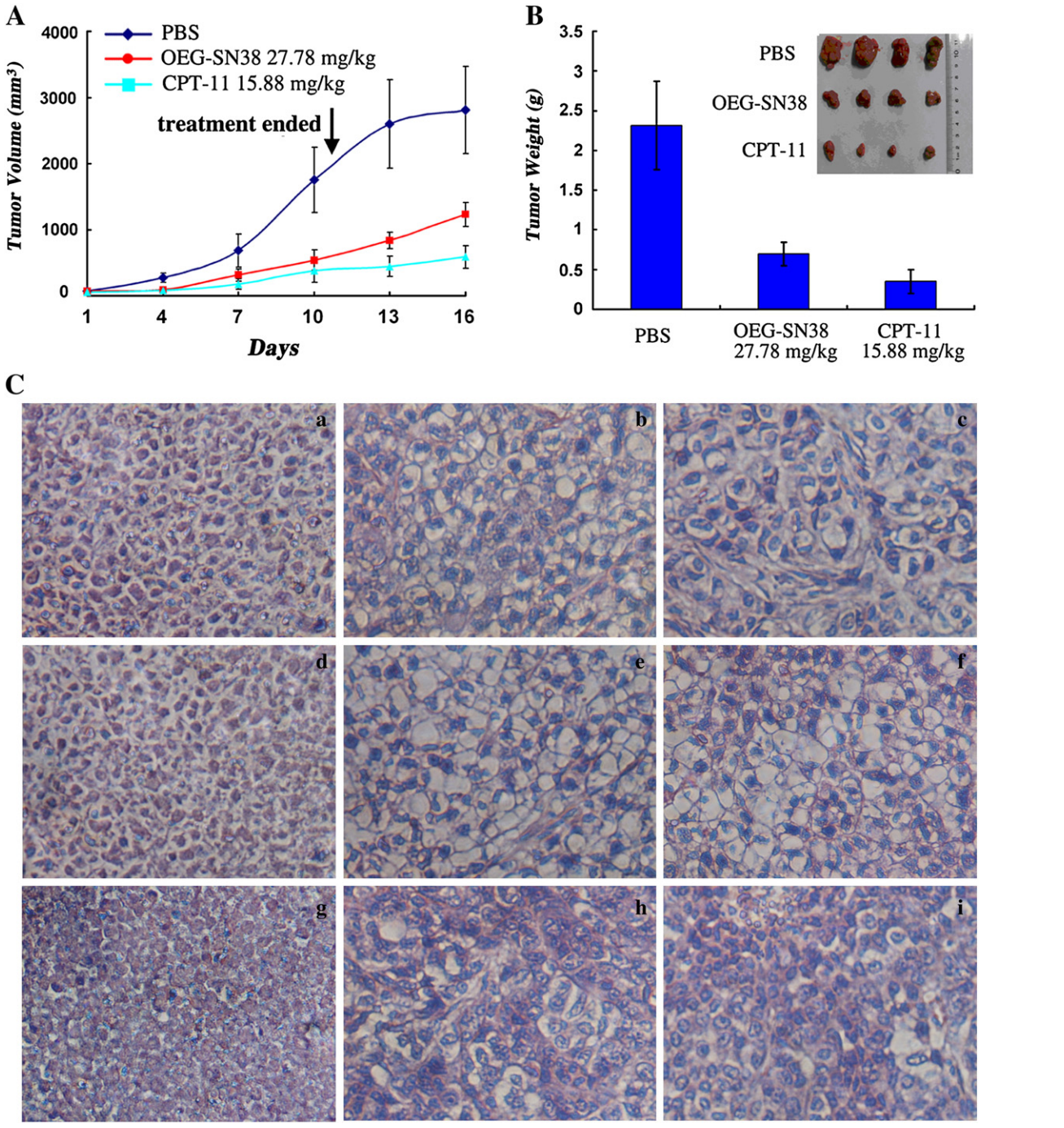

Fig. 7. Therapeutic effects of OEG-SN38 and CPT-11 against SKOV-3 human ovarian xenograft tumors and representative histological features of BCap37 and SKOV-3 tumor tissue sections. Nude mice bearing SKOV-3 tumors were treated with PBS, OEG-SN38 or CPT-11 (q2d×6). 13.89 mg/kg OEG-SN38 and 7.94 mg/kg CPT-11 were equivalent to 5 mg/kg SN38. 27.78 mg/kg OEG-SN38 and 15.88 mg/kg CPT-11 were equivalent to 10 mg/kg SN38. A, determination of tumor volume. B, tumor weight upon animal termination. Data were presented as Mean ± S.E. Insert, photos of tumors upon animal termination. C, H&E staining of tumor tissue sections. a–f: BCap37 tumors treated with PBS (a, d), 7.94 mg/kg CPT-11 (b), 13.89 mg/kg OEG-SN38 (c), 15.88 mg/kg CPT-11 (e) and 27.78 mg/kg OEG-SN38 (f); g–i: SKOV-3 tumor treated with PBS (g), 15.88 mg/kg CPT-11 (h) and 27.78 mg/kg OEG-SN38 (i). Tumors treated with OEG-SN38 or CPT-11 showed enlarged size of tumor cells, decreased cellularity and more apoptotic cells containing small nuclear fragments surrounded by a narrow rim of cytoplasm when compared with control groups. Magnification, ×40.

dissolved in DMSO, but significantly better than CPT-11, against a large panel of tumor cells. Moreover, OEG-SN38 was proven to cause apparent G2/M arrest in cancer cells. These data suggested that SN38 was effectively released from its prodrug once inside tumor cells and was available to inhibit or kill tumor cells. In contrast, tumor cells were significantly less sensitive to CPT-11-induced cell cycle arrest and cell death. Free SN38 exhibited relatively better *in vitro* antitumor activity and superior ability to induce cell cycle arrest in comparison with OEG-SN38, and this might be due to the fact that SN38 firstly needs to be released from the prodrug before acting on tumor cells.

Another obstacle linked to CPT-11 clinical utility is its dose limiting toxicity, *e.g.* severe gastrointestinal toxicity and myelosuppression. Particularly, the high interpatient variability in both efficacy and toxicity after administration of CPT-11 significantly interfere with its safety for the treatment of cancer patients. In this study, we also determined

the LD_{50} of newly synthesized OEG-SN38, and found that the LD_{50} of OEG-SN38 (151.36 mg/kg) was around 11-fold higher than the effective dosage of OEG-SN38 (equivalent to 5 mg/kg SN38), indicating that low toxicities to normal tissues and high safety are associated with OEG-SN38. Further studies with both human breast and ovarian xenograft tumor models demonstrated that OEG-SN38 exhibited impressive *in vivo* antitumor activity without detectable toxicity. Although CPT-11 also demonstrated remarkable antitumor activity in tumor-bearing mice, previous investigations have revealed that there exists great interspecies variability in CPT-11 activation in rodents and humans [33]. For instance, CPT-11 is converted to its active component SN38 rapidly in rodents, and followed by high initial plasma SN38 concentrations because of the abundant plasma carboxylesterase [34–36]. However, much less SN38 was initially detected in patients infused with single high-dose CPT-11 due to lack of carboxylesterase in human plasma [36,37]. Meanwhile, approximately 50% of injected CPT-11 could be converted to SN38 in rodents, while this ratio is far exceeded that in humans (only around 2-8%) [7,34]. Hence, high therapeutic index of CPT-11 in rodents does not identify with that in humans. On the other hand, large amounts of other esterases including butyrylcholinesterase, paraoxonase and albumin esterase were observed in humans, which would permit the ester bond of OEG-SN38 to be hydrolyzed and release active SN38, thus bypassing carboxylesterase-mediated activation for CPT-11 [36]. Therefore, we believe that the injection of OEG-SN38 in cancer patients would allow tumor sites to be exposed to active SN38 at a high concentration more easily and selectively, which may lead to better therapeutic efficacy of OEG-SN38 than CPT-11 in humans. Histological analysis of tumor tissues further confirmed the effectiveness of OEG-SN38 in inhibiting tumor growth and inducing tumor cell apoptotic cell death *in vivo*.

Conclusion

In this study, we successfully designed and synthesized a novel type of SN38-incorporating nanoparticles, OEG-SN38, aiming to overcome not only various drawbacks of CPT-11 and SN38, but also various limitations of reported SN38-incorporating drug delivery systems, especially low drug loading and premature drug release. OEG-SN38 demonstrated dramatically high and stable drug loading, significantly improved solubility, stability and released active SN38 in a controlled manner. Further studies indicate that OEG-SN38 nanoparticles exhibited excellent antitumor activities against a large panel of cultured tumor cell lines, and showed favorable therapeutic effect and low toxicities to normal tissues in tumor-bearing mice. OEG-SN38 holds the promise to become a chemotherapeutic drug better than CPT-11, and deserves further preclinical and clinical development.

Acknowledgments

The authors thank the NSFC-21090352, NSFC-21104065, NSFC-21274125, National Fund for Distinguished Young Scholars (50888001), Public welfare project of Zhejiang Province (2011C21055), ZJ-DST-2011C21055, ZJNSF-Y2090386, and joint project of Zhejiang Province and Ministry of Health (WKJ20092024).

Appendix A. Supplementary data

Supplementary data to this article can be found online at http://dx.doi.org/10.1016/j.jconrel.2012.12.019.

References

[1] R.H.J. Mathijssen, R.J. van Alphen, J. Verweij, W.J. Loos, K. Nooter, G. Stoter, A. Sparreboom, Clinical pharmacokinetics and metabolism of irinotecan (CPT-11), Clin. Cancer Res. 7 (2001) 2182–2194.
[2] K. Yoshimatsu, H. Yokomizo, T. Fujimoto, A. Umehara, T. Otani, A. Matsumoto, G. Osawa, K. Ogawa, Pilot study of simplified low-dose S-1 plus CPT-11 as first-line chemotherapy for patients with advanced colorectal cancer, Anticancer Res. 27 (2007) 1657–1661.
[3] L.J.M. Oostendorp, P.F. Stalmeier, P.C. Pasker-de Jong, W.T. Van der Graaf, P.B. Ottevanger, Systematic review of benefits and risks of second-line irinotecan monotherapy for advanced colorectal cancer, Anti-Cancer Drugs 21 (2010) 749–758.
[4] J.G. Slatter, P. Su, J.P. Sams, L.J. Schaaf, L.C. Wienkers, Bioactivation of the anticancer agent CPT-11 to SN-38 by human hepatic microsomal carboxylesterases and the *in vitro* assessment of potential drug interactions, Drug Metab. Dispos. 25 (1997) 1157–1164.
[5] G.G. Chabot, Clinical pharmacokinetics of irinotecan, Clin. Pharmacokinet. 33 (1997) 245–259.
[6] V. Charasson, M.C. Haaz, J. Robert, Determination of drug interactions occurring with the metabolic pathways of irinotecan, Drug Metab. Dispos. 30 (2002) 731–733.
[7] P.D. Senter, K.S. Beam, B. Mixan, A.F. Wahl, Identification and activities of human carboxylesterases for the activation of CPT-11, a clinically approved anticancer drug, Bioconjug. Chem. 12 (2001) 1074–1080.
[8] N.F. Smith, W.D. Figg, A. Sparreboom, Pharmacogenetics of irinotecan metabolism and transport: an update, Toxicol. in Vitro 20 (2006) 163–175.
[9] H. Bleiberg, CPT-11 in gastrointestinal cancer, Eur. J. Cancer 35 (1999) 371–379.
[10] P. Sapra, H. Zhao, M. Mehlig, J. Malaby, P. Kraft, C. Longley, L.M. Greenberger, I.D. Horak, Novel delivery of SN38 markedly inhibits tumor growth in xenografts, including a camptothecin-11 — refractory model, Clin. Cancer Res. 14 (2008) 1888–1896.
[11] Y. Matsumura, Preclinical and clinical studies of NK012, an SN-38-incorporating polymeric micelles, which is designed based on EPR effect, Adv. Drug Deliv. Rev. 63 (2011) 184–192.
[12] A. Pal, S. Khan, Y.F. Wang, N. Kamath, A.K. Sarkar, A. Ahmad, S. Sheikh, S. Ali, D. Carbonaro, A. Zhang, I. Ahmad, Preclinical safety, pharmacokinetics and antitumor efficacy profile of liposome-entrapped SN-38 formulation, Anticancer Res. 25 (2005) 331–341.
[13] N. Vijayalakshmi, A. Ray, A. Malugin, H. Ghandehari, Carboxyl-Terminated PAMAM-SN38 Conjugates: Synthesis, Characterization, and in Vitro Evaluation, Bioconjug. Chem. 21 (2010) 1804–1810.
[14] Y.Q. Shen, E.L. Jin, B. Zhang, C.J. Murphy, M.H. Sui, J. Zhao, J.Q. Wang, J.B. Tang, M.H. Fan, E. Van Kirk, W.J. Murdoch, Prodrugs forming high drug loading multifunctional nanocapsules for intracellular cancer drug delivery, J. Am. Chem. Soc. 132 (2010) 4259–4265.
[15] A. Gomez-Hens, J.M. Fernandez-Romero, Analytical methods for the control of liposomal delivery systems, TrAC, Trends Anal. Chem. 25 (2006) 167–178.
[16] H.D. Tang, C.J. Murphy, B. Zhang, Y.Q. Shen, M.H. Sui, E.A. Van Kirk, X.W. Feng, W.J. Murdoch, Amphiphilic curcumin conjugate-forming nanoparticles as anticancer prodrug and drug carriers: *in vitro* and *in vivo* effects, Nanomedicine 5 (2010) 855–865.
[17] H. Zhao, C. Lee, P.K. Sai, Y.H. Choe, M. Boro, A. Pendri, S.Y. Guan, R.B. Greenwald, 20-O-acylcamptothecin derivatives: evidence for lactone stabilization, J. Org. Chem. 65 (2000) 4601–4606.
[18] J. Yang, W.W. Liu, M.H. Sui, J.B. Tang, Y.Q. Shen, Platinum (IV)-coordinate polymers as intracellular reduction-responsive backbone-type conjugates for cancer drug delivery, Biomaterials 32 (2011) 9136–9143.
[19] M.H. Sui, J.M. Dziadyk, X.M. Zhu, W.M. Fan, Cell cycle-dependent antagonistic interactions between paclitaxel and gamma-radiation in combination therapy, Clin. Cancer Res. 10 (2004) 4848–4857.
[20] M.H. Sui, F. Chen, Z. Chen, W.M. Fan, Glucocorticoids interfere with therapeutic efficacy of paclitaxel against human breast and ovarian xenograft tumors, Int. J. Cancer 119 (2006) 712–717.
[21] M. Sui, Y. Huang, B.H. Park, N.E. Davidson, W. Fan, Estrogen receptor alpha mediates breast cancer cell resistance to paclitaxel through inhibition of apoptotic cell death, Cancer Res. 67 (2007) 5337–5344.
[22] E. Blanco, A. Hsiao, A.P. Mann, M.G. Landry, F. Meric-Bernstam, M. Ferrari, Nanomedicine in cancer therapy: innovative trends and prospects, Cancer Sci. 102 (2011) 1247–1252.
[23] P.Y. Lee, K.K.Y. Wong, Nanomedicine: a new frontier in cancer therapeutics, Curr. Drug Deliv. 8 (2011) 245–253.
[24] A. Carie, J. Rios-Doria, T. Costich, B. Burke, R. Slama, H. Skaff, K. Sill, IT-141, a polymer micelle encapsulating SN-38, induces tumor regression in multiple colorectal cancer models, J. Drug Deliv. 2011 (2011) 869027.
[25] H. Maeda, J. Wu, T. Sawa, Y. Matsumura, K. Hori, Tumor vascular permeability and the EPR effect in macromolecular therapeutics: a review, J. Control. Release 65 (2000) 271–284.
[26] L. Brannon-Peppas, J.O. Blanchette, Nanoparticle and targeted systems for cancer therapy (vol 56, pg 1649, 2004), Adv. Drug Deliv. Rev. 61 (2009) 364.
[27] L. Brannon-Peppas, J.O. Blanchette, Nanoparticle and targeted systems for cancer therapy, Adv. Drug Deliv. Rev. 56 (2004) 1649–1659.
[28] H.W. Wang, T.B. Shrestha, M.T. Basel, R.K. Dani, G.M. Seo, S. Balivada, M.M. Pyle, H. Prock, O.B. Koper, P.S. Thapa, D. Moore, P. Li, V. Chikan, D.L. Troyer, S.H. Bossmann, Magnetic-Fe/Fe3O4-nanoparticle-bound SN38 as carboxylesterase-cleavable prodrug for the delivery to tumors within monocytes/macrophages, Beilstein J. Nanotechnol. 3 (2012) 444–455.
[29] M.T. Basel, S. Balivada, T.B. Shrestha, G.M. Seo, M.M. Pyle, M. Tamura, S.H. Bossmann, D.L. Troyer, A cell-delivered and cell-activated SN38-dextran prodrug increases survival in a murine disseminated pancreatic cancer model, Small 8 (2012) 913–920.
[30] G.M. Seo, R.S. Rachakatla, S. Balivada, M. Pyle, T.B. Shrestha, M.T. Basel, C. Myers, H.W. Wang, M. Tamura, S.H. Bossmann, D.L. Troyer, A self-contained enzyme

activating prodrug cytotherapy for preclinical melanoma, Mol. Biol. Rep. 39 (2012) 157–165.
[31] S.G. Arbuck, C.H. Takimoto, An overview of topoisomerase I — targeting agents, Semin. Hematol. 35 (1998) 3–12.
[32] W.H. Zhang, A. Poh, A.A. Fanous, A. Eastman, DNA damage-induced S phase arrest in human breast cancer depends on Chk1, but G(2) arrest can occur independently of Chk1, Chk2 or MAPKAPK2, Cell Cycle 7 (2008) 1668–1677.
[33] F. Meyer-Losic, C. Nicolazzi, J. Quinonero, F. Ribes, M. Michel, V. Dubois, C. de Coupade, M. Boukaissi, A.S. Chene, I. Tranchant, V. Arranz, I. Zoubaa, J.S. Fruchart, D. Ravel, J. Kearsey, DTS-108, a novel peptidic prodrug of SN38: *in vivo* efficacy and toxicokinetic studies, Clin. Cancer Res. 14 (2008) 2145–2153.
[34] W.C. Zamboni, C.F. Stewart, P.J. Cheshire, L.B. Richmond, S.K. Hanna, X.L. Luo, C. Poquette, J.P. McGovren, J.A. Houghton, P.J. Houghton, Studies of the efficacy and pharmacology of irinotecan against human colon tumor xenograft models, Clin. Cancer Res. 4 (1998) 743–753.
[35] W.C. Zamboni, P.J. Houghton, J. Thompson, P.J. Cheshire, S.K. Hanna, L.B. Richmond, X.L. Lou, C.F. Stewart, Altered irinotecan and SN-38 disposition after intravenous and oral administration of irinotecan in mice bearing human neuroblastoma xenografts, Clin. Cancer Res. 4 (1998) 455–462.
[36] B. Li, M. Sedlacek, I. Manoharan, R. Boopathy, E.G. Duysen, P. Masson, O. Lockridge, Butyrylcholinesterase, paraoxonase, and albumin esterase, but not carboxylesterase, are present in human plasma, Biochem. Pharmacol. 70 (2005) 1673–1684.
[37] L.P. Rivory, M.C. Haaz, P. Canal, F. Lokiec, J.P. Armand, J. Robert, Pharmacokinetic interrelationships of irinotecan (CPT-11) and its three major plasma metabolites in patients enrolled in phase I/II trials, Clin. Cancer Res. 3 (1997) 1261–1266.